Proceedings of the Korean Nuclear Society Spring Meeting
Gyeongju, Korea, 2004

Fluidelastic Instability and Fretting-Wear Characteristics of Steam Generator Helical Tubes Subjected to Single-Phase External Flow and Two-Phase Internal Flow

Jong Chull Jo, Myung Jo Jhung, Woong Sik Kim and Hho Jung Kim
Korea Institute of Nuclear Safety
19 Guseong-dong, Yuseong-gu, Daejeon 305-338 Korea

Abstract

This study investigates the fluidelastic instability characteristics of steam generator (SG) helical type tubes and the safety assessment of the potential for fretting-wear damages caused by foreign object in operating nuclear power plants. The thermal-hydraulic conditions of both tube side and shell side flow fields are predicted by a general purpose computational fluid dynamics code employing the finite volume element modeling. To get the natural frequency, corresponding mode shape and participation factor, modal analyses are performed for helical type tubes with various conditions. Special emphases are on the effects of coil diameter and the number of turns on the modal and instability characteristics of tubes, which are expressed in terms of the natural frequency, corresponding mode shape and stability ratio. Also, the wear rate of helical type tube caused by foreign object is calculated using the Archard formula and the remaining life of the tube is predicted, and discussed in this study is the effect of the flow velocity and vibration of the tube on the remaining life of the tube. In addition, addressed is the effect of the external pressure on the vibration and fretting-wear characteristics of the tube.

1. Introduction

Advanced nuclear power reactors are currently under development worldwide. Some designs are now ready for construction. One advantage of the advanced type of reactor is the easy implementation of advanced design concepts and technology. Drastic safety enhancement can be achieved by adopting inherent safety characteristics and passive safety features. Economic improvement is pursued through system simplification, modularization and reduction in construction time.

SMART (System-integrated Modular Advanced ReacTor), a small sized integral type PWR is one of those advanced types of reactors, which is being developed in Korea. All the major primary components are contained in a single pressurized vessel. The in-vessel self-controlling pressurizer is one of the advanced design features. The system pressure is passively adjusted by partial pressure of steam and nitrogen gas filled in the pressurizer in accordance with variation in pressure and temperature of the primary coolant. The control element drive mechanism has a very fine-step maneuvering capability to compensate for the core reactivity change caused by fuel depletion during normal operation. The modular type once-through SG has an innovative design feature with helically coiled tubes to produce superheated steam at normal operating condition.

There are twelve identical SG cassettes which are located on the annulus formed by the reactor pressure vessel and the core support barrel. Each SG cassette is of once-through design with a number of helically coiled tubes. The primary reactor coolant flows downward in the shell side of the SG tubes, while the secondary feedwater flows upward in the tube side.

The helical type tubes adopted for SMART may have a totally different behavior from that of U-tubes which are used in typical PWR (Jo and Shin, 1999, Jo et al., 2003a, 2003b). It necessitates a study on fluidelastic instability and fretting-wear prediction including vibration characteristics to assure the structural integrity of the helically coiled tubes during normal operation.

The problem of steam generator tube rupture (SGTR) in operating nuclear power plants has been one of the most significant safety issue worldwide for a long time. This is because leakage due to SGTR has such serious implications as possible direct release of radioactive fission products to the environment and the loss of coolant.

Tube vibration excited by dynamic forces of external fluid flow in nuclear steam generators may either initiate such mechanical damages on intact tubes as fretting-wear and fatigue, which may eventually result in severe tube failures or accelerate the growth of pre-existing flaw or crack caused by stress corrosion in the tubes.

Even less significant dynamic forces of external fluid flow exerting to tube which can not cause any damage to the intact tube may lead to excessive vibration resulting in fatigue failure of the tube with flaw (crack) which is pre-existed or growing one due to stress-corrosion or in failure of the tube due to fretting-wear. Therefore, with regard to nuclear safety it is very important to assess the potential for SG tube failures due to fluidelastic instability or fretting-wear and take the necessary preventive measures for minimizing the probability of SG tube failures in operating plants. The assessment of the potential for such a SG tube failure can be accomplished by performing a fluidelastic instability analysis for susceptible tubes or the fretting-wear analysis by foreign object, for which the prerequisite is the performance of the modal analysis.

This study investigates the fluidelastic instability and fretting-wear characteristics of steam generator helical tubes. To do this, thermal-hydraulic conditions of both tube side and shell side flow fields are predicted by a general purpose computational fluid dynamics code employing the finite volume element modeling. In addition, modal analyses are performed for the finite element modelings of tubes with various conditions. The effects of coil diameter, the number of turns, the number of supports and the status of inner fluid on the modal, fluidelastic instability and fretting-wear characteristics of tubes, which are expressed in terms of the natural frequency, corresponding mode shape, stability ratio and time required to wear the tube are investigated. Also, addressed in this study is the effect of the external pressure on the vibration, fluidelastic instability and fretting-wear characteristics of the tube.

2. Analysis

2.1 Thermal-hydraulic Analysis

The conceptual schematic diagram of a helical coil steam generator is shown in Fig. 1. The single steam generator cassette is a kind of once-through heat exchanger with helically coiled tubes. During the normal reactor operation, each cassette produces highly superheated steam from the outlet of the helically coiled tubes by heat exchange between the highly pressurized hot fluid (light water) flowing downward through the shell side (outside of the tubes) and the cold fluid flowing upward through the inside of tubes at lower pressure.

Due to the heat transfer, the cold feedwater entering the tube side is heated up. When it reaches the saturation temperature at the specified pressure, boiling occurs. Initially, bubbles form along the tube walls and a two-phase flow occurs. With a large amount of heat transferred continuously from the outside of tubes, the fluid will evaporate completely and finally the evaporated steam will be superheated within the temperature limit not exceeding the temperature of the primary fluid at the shell side.

For the modal analysis and shell side flow-induced fluidelastic instability assessment of such a helically coiled tube, the density distributions along the tube for both internal and external fluids and the cross-flow tube gap velocity distribution along the tube have to be known as a requisite.

As can be imagined, the geometrical configuration of helical tube bundle inside the practical nuclear steam generator is very complex and the thermal phase change occurs at tube side instead of shell side contrary to the case of conventional nuclear steam generators.

These make the thermal-hydraulic analysis of such helically coiled steam generators difficult. Therefore, in this study, a simplified model of helically coil type steam generator tube is designed for the use in the thermal-hydraulic analysis as shown in Fig. 2.

Both tube side and shell side flow fields are simulated using the general purpose computational fluid dynamics code CFX-5.6 (2003) employing the finite volume element modeling. The internal and external flows are simulated using the standard k–ε turbulent model and the solution domain of fluid flow and heat transfer including the conducting solid tube wall is calculated employing the conjugate heat transfer analysis approach. Especially, for the calculation of tube side multiphase flow accompanying the thermal phase change (boiling), inhomogeneous two-fluid model is used.

The Reynolds averaged governing equations for conservation of mass, momentum, energy, and turbulent quantities for the present problem in a Cartesian coordinate system can be expressed as follows;

Mass conservation of phase-α

$$\frac{\partial}{\partial t}\left(r_\alpha \rho_\alpha\right) + \nabla \cdot \left(r_\alpha \rho_\alpha U_\alpha\right) = \sum_{\beta=1}^{N}\left(\Gamma_{\alpha\beta}^{+} - \Gamma_{\beta\alpha}^{+}\right) \tag{1}$$

where r_α, ρ_α and U_α present the volume fraction, density, and velocity of phase-α, respectively. In addition, N denotes the total number of phases and $\Gamma_{\alpha\beta}^{+}$ stands for the positive mass flow rate per unit volume from phase β to phase α. The mathematical notation $\nabla \cdot V$ means the divergence of a vector $V(=\partial V_x / \partial x + \partial V_y / \partial y + \partial V_z / \partial z)$.

The summation of volume fraction is 1.

$$\sum_{\alpha} r_{\alpha} = 1 \tag{2}$$

Momentum conservation of phase-α

$$\frac{\partial}{\partial t}\left(r_{\alpha}\rho_{\alpha}U_{\alpha}\right) + \nabla\cdot\left(r_{\alpha}\rho_{\alpha}U_{\alpha}\otimes U_{\alpha}\right) - \nabla\cdot\left(r_{\alpha}\mu_{\alpha eff}\left(\nabla U_{\alpha} + (\nabla U_{\alpha})^{T}\right)\right) = -r_{\alpha}\nabla p'_{\alpha} + r_{\alpha}(\rho_{\alpha} - \rho_{ref})g + M_{\alpha} \tag{3}$$

where

$$p'_{\alpha} = p_{\alpha} + \frac{2}{3}\rho_{\alpha}k_{\alpha} \tag{4}$$

$$\mu_{\alpha eff} = \mu_{\alpha} + \mu_{t\alpha} \tag{5}$$

$$\mu_{t\alpha} = C_{\mu}\rho_{\alpha}\left(\frac{k_{\alpha}^{2}}{\varepsilon_{\alpha}}\right) \tag{6}$$

and μ_{α}, p_{α}, k_{α} and ε_{α} represent viscosity, pressure, turbulence kinetic energy, and turbulence dissipation rate of phase-α, respectively. C_{μ} is a constant given as 0.09. The operator $\otimes$ is a tensor product and $(\nabla U_{\alpha})^{T}$ is the transpose of a matrix ∇U_{α}.

M_{α} denotes the sum of interfacial forces acting on phase-α due to the presence of other phases i.e., drag forces and momentum transfer associated with inter-phase mass transfer, which is expressed as,

$$M_{\alpha} = \sum_{\beta\neq\alpha} M_{\alpha\beta} = \sum_{\beta=1}^{N} c_{\alpha\beta}^{(d)}(U_{\beta} - U_{\alpha}) + \sum_{\beta=1}^{N}\left(\Gamma_{\alpha\beta}^{+}U_{\beta} - \Gamma_{\beta\alpha}^{+}U_{\alpha}\right) + \ldots \tag{7}$$

Because all phases share the same pressure field, the pressure constraint is given as,

$$p_{\alpha} = p \quad \text{for all} \quad \alpha = 1, 2, \ldots\ldots\ldots, N. \tag{8}$$

Energy conservation of phase-α

$$\frac{\partial}{\partial t}\left(r_{\alpha}\rho_{\alpha}h_{\alpha}\right) + \nabla\cdot\left(r_{\alpha}\left(\rho_{\alpha}U_{\alpha}h_{\alpha} - \lambda_{\alpha}\nabla T_{\alpha}\right)\right) = \sum_{\beta=1}^{N}\left(\Gamma_{\alpha\beta}^{+}h_{\beta s} - \Gamma_{\beta\alpha}^{+}h_{\alpha s}\right) + Q_{\alpha} \tag{9}$$

where h_{α}, T_{α} and λ_{α} represent the sensible enthalpy, temperature, and thermal conductivity of phase-α, respectively. Q_{α} denotes the total interphase heat per unit volume transferred to phase-α due to the interaction with other phases given as,

$$Q_{\alpha} = \sum_{\beta\neq\alpha} Q_{\alpha\beta} = h_{\alpha\beta}A_{\alpha\beta}(T_{\beta} - T_{\alpha}) \tag{10}$$

And the term $(\Gamma_{\alpha\beta}^{+}h_{\beta s} - \Gamma_{\beta\alpha}^{+}h_{\alpha s})$ represents heat transfer induced by interphase mass transfer.

Transport equations for turbulence kinetic energy and turbulence dissipation rate for phase-α

$$\frac{\partial}{\partial t}\left(r_{\alpha}\rho_{\alpha}k_{\alpha}\right) + \nabla\cdot\left(r_{\alpha}\left(\rho_{\alpha}U_{\alpha}k_{\alpha} - (\mu_{\alpha} + \frac{\mu_{t\alpha}}{\sigma_{k}})\nabla k_{\alpha}\right)\right) = r_{\alpha}(P_{k\alpha} - \rho_{\alpha}\varepsilon_{\alpha}) \tag{11}$$

$$\frac{\partial}{\partial t}\left(r_{\alpha}\rho_{\alpha}\varepsilon_{\alpha}\right) + \nabla\cdot\left(r_{\alpha}\left(\rho_{\alpha}U_{\alpha}\varepsilon_{\alpha} - (\mu_{\alpha} + \frac{\mu_{t\alpha}}{\sigma_{\varepsilon}})\nabla\varepsilon_{\alpha}\right)\right) = r_{\alpha}\frac{\varepsilon_{\alpha}}{k_{\alpha}}(C_{\varepsilon 1}P_{k\alpha} - C_{\varepsilon 2}\rho_{\alpha}\varepsilon_{\alpha}) \tag{12}$$

where $C_{\varepsilon 1}$, $C_{\varepsilon 2}$, σ_{k} and σ_{ε} are constants having the values of 1.44, 1.92, 1.0, and 1.3, respectively. $P_{k\alpha}$ is the turbulence production for the phase-α due to viscous and buoyancy forces modelled as,

$$P_{k\alpha} = \mu_{t\alpha}\nabla U_{\alpha}\cdot(\nabla U_{\alpha} + \nabla U_{\alpha}^{T}) - \frac{2}{3}\nabla\cdot U_{\alpha}(3\mu_{t\alpha}\nabla\cdot U_{\alpha} + \rho_{\alpha}k_{\alpha}) + P_{kb\alpha} \tag{13}$$

where $P_{kb\alpha}$ is the buoyancy production term for the phase- α and is given for the full buoyancy model as,

$$P_{kb\alpha} = \frac{\mu_{\alpha t}}{\mathrm{Pr}_{t\alpha}} g \cdot \nabla \rho_{\alpha} \tag{14}$$

Thermal phase change model

The mass flux into phase-α from phase β, $\dot{m}_{\alpha\beta}$ is given as,

$$\dot{m}_{\alpha\beta} = \frac{q_{\alpha s} + q_{\beta s}}{H_{\beta s} - H_{\alpha s}} \tag{15}$$

where $q_{\alpha s}$ and $q_{\beta s}$ are the sensible heat flux to phase-α from the interface and that to phase-β, respectively. $H_{\alpha s}$ and $H_{\beta s}$ represent interfacial values of enthalpy carried into and out of the phases due to phase change, respectively.

Boundary conditions

The boundary conditions used in the present study are those provided by CFX-5.6. The wall function method is used for the tube wall boundary conditions and free slip and adiabatic boundary conditions are assumed for both inner and outer wall surfaces of shell-side fluid column which has the shape of hollow circular cylinder with finite wall (fluid) thickness. The inlet conditions are prescribed as,

$$U_{\alpha} = U_{\alpha,in},\ T_{\alpha} = T_{\alpha,in},\ k_{\alpha} = k_{\alpha,in},\ \varepsilon_{\alpha} = \varepsilon_{\alpha,in} \tag{16}$$

at the inlet of either tube or shell.
Wall functions at the inner and outer surfaces of pipe wall are used.

$$\frac{\partial u_{\alpha 1}}{\partial n} = \frac{\partial u_{\alpha 2}}{\partial n} = \frac{\partial u_{\alpha 3}}{\partial n} = \frac{\partial T_{\alpha}}{\partial n} = \frac{\partial k_{\alpha}}{\partial n} = \frac{\partial \varepsilon_{\alpha}}{\partial n} = 0 \tag{17}$$

at the inner and outer surfaces of the shell-side fluid column which has the shape of hollow circular cylinder with finite wall (fluid) thickness

$$\frac{\partial T_{\alpha}}{\partial n} = \frac{\partial k_{\alpha}}{\partial n} = \frac{\partial \varepsilon_{\alpha}}{\partial n} = 0 \tag{18}$$

at the outlet open surface of either tube or shell.
In addition, the velocity components are adjusted to satisfy the overall mass conservation at the outlet of either tube or shell.

For the SG thermal-hydraulic analysis using CFX-5.6, the solution domain is divided into a finite number of hexahedral control volume cells and the total number of cells used in the calculation is around 600,000, which was determined considering the result of mesh sensitivity study as well as the computation efficiency.

2.2 Modal Analysis

Modal analyses using a commercial computer code ANSYS 7.0 (2003) are performed to find the vibration characteristics of the tube. Several different kinds of finite element models are developed according to the coil diameter, full height, the number of turns (helix angle) and the number of support points (Table 1).

Finite element models are developed using the elastic straight pipe elements (PIPE16) for the helical tube and 3-D point-to-point contact elements (CONTAC52) between support and tube. PIPE16 is a uniaxial element with tension-compression, torsion, and bending capabilities. CONTAC52 represents two surfaces which may maintain or break physical contact and may slide relative to each other. The element is capable of supporting only compression in the direction normal to the surfaces and shear (Coulomb friction) in the tangential direction. The finite element model consists of 1280 PIPE16 elements for the helical tube and 65 CONTAC52 elements between support and tube for eight support points Type A as shown in Fig. 3.

The boundary conditions at the two ends of the tube are fixed. To simulate the nodes of the tube at the support locations to be free to move in the longitudinal direction, contact elements are used between support and corresponding tube locations with the support node fixed.

The Block Lanczos method is used for the eigenvalue and eigenvector extractions to calculate 50 natural frequencies. It uses the Lanczos algorithm where the Lanczos recursion is performed with a block of vectors. This method is as accurate as the subspace method, but faster. The Block Lanczos method is especially powerful when searching for eigenfrequencies in a given part of the eigenvalue spectrum of a given system. The convergence rate of the eigenfrequencies will be about the same when extracting modes in the midrange and higher end of the spectrum as when extracting the lowest modes.

2.3 Fluidelastic Instability Assessment

The critical velocity to initiate fluidelastic instability was formulated by Connors (1981) for the simple case of a tube bank subjected to uniform cross flow over the entire length of the tubes. The formulation of fluidelastic instability proposed by Connors is a semi-empirical correlation fitted by experimental data and is expressed in terms of a dimensionless flow velocity called a reduced velocity $v_{c,n} / f_n d$ and a dimensionless mass-damping parameter $2\pi\zeta_t m_t / \rho d^2$ as follows ;

$$\frac{v_{c,n}}{f_n d} = C\left(\frac{2\pi\zeta_t m_t}{\rho d^2}\right)^{0.5} \tag{19}$$

where $v_{c,n}$, C, f_n, ρ and d are the critical velocity of the nth free vibration mode, the fluidelastic instability coefficient (or the Connors' constant), the natural frequency of the nth mode, the shell-side fluid density and the outer diameter of tube, respectively. Also, ζ_t and m_t are the total damping ratio and the total mass per unit length of the tube.

The total damping ratio in two-phase flow is the sum of viscous damping, support damping and two-phase damping and they may be determined either from available measured data or by empirical expressions. Because of much difficulty from an experimental point of view, only limited data on the damping in two-phase flows are available at present. Au-Yang (2001) recommended a mean damping ratio for water or wet steam for tightly supported tube and loosely supported tube as 0.015 and 0.05, respectively.

The total effective mass of a tube surrounded by a fluid consists of three components; mass of the tube material, mass of fluid in the tube and added mass (or hydrodynamic mass) of fluid displaced by the tube. The third component of the effective tube mass is affected by the proximity of other tubes in the tube bundle and it is bounded by the pitch pattern for maximum and minimum by the triangular and square pitch, respectively .

The fluidelastic instability coefficient C is a function of the tube arrangement and the ratio of tube pitch p over the outer diameter of tube d. Mean values for the onset of instability can be established by fitting semi-empirical correlation to experimental data and they are shown in Table 2 (ASME 1998). For the entire mass-damping parameter range, mean value of C = 3.3 was recommended by Pettigrew and Gorman (1981) and Paidoussis (1983). Also Yetisir and Pettigrew (2001) used C = 3 for $p / d \geq 1.47$ and $C = 4.76\ (p - d) / p + 0.76$ for $p / d < 1.47$ as a bounding design guideline.

The critical velocity $v_{c,n}$ is related to the gap velocity v_g between the tubes, which is determined based on the tube pitch and diameter as applied to the approach or free stream velocity v_∞. The gap velocity in the fluid region is defined as

$$v_g = \frac{p}{p-d} v_\infty \tag{20}$$

For most practical shell-and-tube type heat exchangers including SGs, the tube bundles consist of multi-span tubes and only partial portions of the tubes may be exposed to cross flow. The onset of fluidelastic instability of multi-span tubes partially subjected to cross flow may be predicted by several approaches. It has been indicated that the equivalent velocity approach based on mode shapes is valid and the simplest one to use (Eisinger et al., 1989). Equation (19) was originally extended by Eisinger and Juliano (1975) for the use of equivalent velocity approach in the fluidelastic instability analysis for the tubes partially subjected to cross flow.

The fluidelastic instability for tubes partially exposed to cross flow can be evaluated by the comparison of the critical velocity $v_{c,n}$ with the effective cross flow gap velocity v_{ge} which is a uniform cross flow velocity equivalent to the actual non-uniform normal-to-tube cross flow gap velocity distribution along the tube length $v_g(x)$, where x denotes the distance along the tube with full length from the hot side tube end.

$v_{ge,n}$ is a variable depending on the free vibration mode as in the case of $v_{c,n}$. The value of $v_{ge,n}$ equivalent to $v_g(x)$ can be determined by weighting the nth mode shape as follows ;

$$v_{ge,n}^{\ 2} = \frac{\frac{1}{\rho_o}\int_0^l \rho(x) v_g^{\ 2}(x) \varphi_n^{\ 2}(x) dx}{\frac{1}{m_o}\int_0^l m_t(x) \varphi_n^{\ 2}(x) dx} \tag{21}$$

where $\varphi_n(x)$ is the nth mode shape function, $\rho(x)$, $m_t(x)$ are the shell-side fluid mass and total tube mass densities along the tube and ρ_o, m_o are the corresponding average densities.

The stability ratio $R_{s,n}$ is defined by the ratio of $v_{ge,n}$ over $v_{c,n}$ as given by

$$R_{s,n} = \frac{v_{ge,n}}{v_{c,n}}, \quad n = 1, 2, 3, \ldots \tag{22}$$

where $R_{s,n}$ indicates the stability ratio for the nth vibration mode. The maximum value among the stability ratios for all vibration modes of a specified tube is used as the criteria to assess the potential instability of the tube. If the maximum value of stability ratio R_s is smaller than unity, the tube is fluidelastically stable. Otherwise, it is unstable and its vibration amplitude becomes divergent rapidly as R_s increases beyond unity, which means that v_{ge} should be less than v_c for all modes during normal operation.

2.4 Fretting-Wear Prediction

Connors (1981) investigated various ways of evaluating and correlating tube wear to tube motion and showed that the Archard's equation (Archard and Hirst, 1956) for adhesive wear can be applied to fretting-wear as well as continuous sliding conditions.

$$V = K \cdot F_n \cdot L \tag{23}$$

where V = volume of wear generated, K = wear coefficient, F_n = normal forces between surfaces and L = total sliding distance. While wear is not theoretically well defined and the Archard's equation is semi-empirical, it has been proved valuable in practical situations. Rubbing motion caused more wear than impacting motion, so Archard's equation can be used to evaluate tube wear due to foreign objects as well as between tube and tube support. Wear coefficients are shown in Fig. 4 for various material combinations from some experimental data (Au-Yang, 2001).

The sliding distance can be calculated with the tube vibration amplitude due to the flow-induced vibration and the tube frequency. The sliding distance per second is four times the product of the tube vibration amplitude and the tube frequency and is calculated as;

$$D = 4 \cdot C * \sqrt{\left(\sum_{m=1}^{n} f_m \cdot d_{m,x} \cdot PF_{m,x}\right)^2 + \left(\sum_{m=1}^{n} f_m \cdot d_{m,y} \cdot PF_{m,y}\right)^2 + \left(\sum_{m=1}^{n} f_m \cdot d_{m,z} \cdot PF_{m,z}\right)^2} \tag{24}$$

where D = sliding distance per second, f_m = mth modal natural frequency of the steam generator tube, $d_{m,x}$ = modal displacement of mode m in x-direction, $d_{m,y}$ = modal displacement of mode m in y-direction, $d_{m,z}$ = modal displacement of mode m in z-direction, $PF_{m,x}$ = modal participation factor of mode m in x-direction, $PF_{m,y}$ = modal participation factor of mode m in y-direction, $PF_{m,z}$ = modal participation factor of mode m in z-direction, and n is the sufficient number of modes that should be considered. Also, C* is the factor which relates the root mean square (RMS) deflection from test or analysis to the amplitude of the modal analysis for a steam generator tube as follows;

$$RMS = C * \sqrt{\left(\sum_{m=1}^{n} d_{m,x} \cdot PF_{m,x}\right)^2 + \left(\sum_{m=1}^{n} d_{m,y} \cdot PF_{m,y}\right)^2 + \left(\sum_{m=1}^{n} d_{m,z} \cdot PF_{m,z}\right)^2} \tag{25}$$

Therefore the total sliding distance L in time t is determined from Eqs. (24) and (25);

$$L = 4t \cdot RMS \cdot \frac{1}{\psi} \tag{26}$$

where

$$\psi = \sqrt{\frac{\left(\sum_{m=1}^{n} d_{m,x} \cdot PF_{m,x}\right)^2 + \left(\sum_{m=1}^{n} d_{m,y} \cdot PF_{m,y}\right)^2 + \left(\sum_{m=1}^{n} d_{m,z} \cdot PF_{m,z}\right)^2}{\left(\sum_{m=1}^{n} f_m \cdot d_{m,x} \cdot PF_{m,x}\right)^2 + \left(\sum_{m=1}^{n} f_m \cdot d_{m,y} \cdot PF_{m,y}\right)^2 + \left(\sum_{m=1}^{n} f_m \cdot d_{m,z} \cdot PF_{m,z}\right)^2}} \tag{27}$$

The wear volume generated on the tube is calculated using Eqs. (23) and (26) as

$$V = 4Kt \cdot RMS \cdot F_n \frac{1}{\psi} \tag{28}$$

The tube depth associated with this wear volume can be determined by defining the geometry of the wear scar. The geometrical relationship between wear volume and wear depth for a SG tube in contact with a flat bar is shown in Fig. 5. Assuming that the tube and flat bar are perfectly aligned, the wear scar volume, V_s, is simply the area of interaction of a straight line and a circle of radius, R, multiplied by the flat bar width, l;

$$V_s = \frac{R^2 l}{2}\left[2\kappa - \sin(2\kappa)\right] \tag{29}$$

where κ is the contact angle (rad) and there is relation between the tube radius R and the wear depth h as

$$\kappa = \cos^{-1}\left(1 - \frac{h}{R}\right) \tag{30}$$

Equating the wear volume generated to the geometrically defined wear volume, the relationship between wear depth and time can be defined. The time required to wear into a tube to the minimum acceptable wall thickness h, which is usually defined as 40% through wall, is calculated from Eqs. (28) and (29) as ;

$$t = \frac{R^2 l \psi}{8KF_n \cdot RMS}[2\kappa - \sin(2\kappa)] \tag{31}$$

Equation (31) was derived based on the assumptions that the foreign object will remain in the same location once the tube wear begins and that only the tube will experience the wear. This can be used to calculate the time required to wear completely through the tube wall. It should be noted that the tube could fail in fatigue before complete wear-through occurred.

3. Results and Discussion

The typical calculation results are suggested in Fig. 6 which shows the density distributions along the tube inside and outsides. As is seen from the Fig. 6, the feedwater entering the tube is heated up, vaporizes, and is superheated in the phase of vapor as the fluid flows upward with the heat input from the hot pressurized water in the shell side. A typical case of the predicted velocity vectors at an inclined vertical cross-section is illustrated in Fig. 7, which shows that the velocity of internal fluid increases significantly due to the phase change while that of external fluid changes hardly because of its incompressibility as can be expected.

Modal analyses for several kinds of finite element models are performed and their results are summarized and typical mode shapes are shown in Figs. 8 through 11.

The effective mass density distribution of the inner fluid along the entire tube is determined from the present thermal-hydraulic analysis as described in the previous work (Jo and Shin, 1999). This mass density is used to find the vibration characteristics. Also the effect of the inner fluid density is investigated by comparing frequencies between three kinds of the steam quality of the inner fluid; water to water, water to steam and steam to steam. The natural frequency variations are shown in Fig. 12 with respect to the quality of the inner fluid. The resulting natural frequency comparisons between the quality of the inner fluid indicate that the frequencies of the water-to-steam case are in the middle of those of steam-to-steam case which have almost the same values of no inner fluid case. As the inner fluid is superheated, the frequencies of the tube increase giving more safety margin for instability. Therefore the inner fluid is assumed to be water-to-steam conservatively.

The support plays a major role to keep the tube from moving freely in all directions. The tube without support is too flexible and has very low frequencies less than 27 Hz for the first 30 modes resulting in critical problems from the standpoint of the fluidelastic instability because the stability ratio is inversely proportional to the frequency as shown in Eqs. (19) and (22). Several supports are installed in the circumferential direction and the effect of support on the frequencies is investigated by comparing frequencies between tubes with and without supports. Support points each turn are 2, 3, 4, 8 and 16 in the circumferential direction. Their natural frequency variations are shown in Fig. 13. The inclusion of supports increases the natural frequencies of the first mode significantly such as from 2.68 Hz of zero support to 705.3 Hz of 8 supports as shown in Fig. 14. Therefore 8 supports for each turn are expected to be enough to avoid the fluidelastic instability by getting high frequencies. Also, less than 8 supports are recommended for tubes with coil diameter less than 422 mm because it is not easy to install supports which need many welding points in difficult working space.

Five different types of helical tubes as shown in Table 1 are chosen to investigate the stability. Modal analyses are performed and their natural frequencies are shown in Fig. 15. The critical velocity for the first mode is calculated from Eq. (19) and is summarized in Figs. 16 and 17. For the tube to be stable fluidelastically, the stability ratio defined in Eq. (22) should be less than unity, which means that the gap velocity should be less than the critical velocity. Therefore the allowable gap velocity is less than the minimum value of the critical velocity shown in Figs. 16 and 17. As shown in Fig. 16, the allowable gap velocity is less than 1.0 m/sec for less than or equal to 3 supports and therefore more than 4 supports are recommended to avoid fluidelastic instability. Also, Fig. 17 shows that Type A is the worst tube for the fluidelastic instability point of view.

The effect of damping on the critical velocity can be predicted from Eq. (19), where the critical velocity is proportional to the square root of the total damping ratio. They are shown in Fig. 18 and damping ratio is found to be significant to determine the critical velocity. Therefore, more accurate estimation of the total damping ratio needs to be made to predict the fluidelastic instability.

The variation of frequencies versus the number of turns and helix angle is given in Figs. 19 and 20, respectively. As the number of turns increases or the helix angle decreases for the same height, the total length of the tube increases and the stiffness of the system decreases when all the other properties are kept the same. The frequencies except for the first several modes are reduced and this is particularly pronounced in the higher modes.

To investigate the effect of the coil diameter on the vibration characteristics of the tube, different diameters are input for Type A. The resulting natural frequencies and their normalized values with respect to the coil diameter of 422 mm are shown in Figs. 21 and 22, which indicate that increasing coil diameter decreases the system stiffness which in turn decreases the frequencies. As the coil diameter is increased, the frequencies get closer each other and coupled modes begin to appear. The normalized natural frequencies can be represented for all modes as;

$$\lambda = 30.70 \cdot \exp\frac{-WD}{93.35} + 0.6733 \tag{32}$$

where λ and WD are the normalized natural frequency and the coil diameter (mm), respectively.

Not like the steam generator U-tubes of typical PWR, the primary side of the coolant flows outside of the tube in SMART and therefore pressure inside of the tube is lower than that of outside. To investigate the effect of the external pressure on the vibration characteristics of the tube, pressure is input as surface load on the element surface of Type A. The resulting natural frequencies are shown in Fig. 23, which indicate that the natural frequency changes are negligible up to about 1000 MPa of the external pressure. Above this pressure, the natural frequencies of some modes jump very rapidly with the increase of the pressure. Considering that the pressure difference during a normal operation of the nuclear power plant is almost 10 MPa, the natural frequency difference can be concluded to be negligible with the inclusion of the pressure. Therefore the effect of external pressure on the remaining life of the tube due to foreign object is expected to be negligible during a normal operation of the nuclear power plant up to the external pressure of about 100 MPa.

ψ defined in Eq. (27) is calculated and summarized in Fig. 24 for five different types of tube from modal analyses results at node 326 where the foreign object is assumed to rest on. Because the time required to wear is proportional to ψ, the remaining life of helical tube with smaller coil diameter decreases significantly comparing that with larger diameter for the same flow velocity (Figs. 24 and 25). It should be noted that tube Type A which has the largest coil diameter has the longest life from the standpoint of fretting-wear even though it was the worst for the fluidelastic instability point of view. For the same situation the helical tubes located in the inner space have smaller coil diameter and experience more fretting-wear than those located in the outer space with larger coil diameter. Therefore it is recommended that actions such as special design or inspection to keep foreign object from remaining in the inner space of SG cassette should be taken.

Figures 24 and 25 show ψ with respect to the total number of modes under consideration, which show that in calculating ψ sufficient number of modes should be considered not to overestimate the remaining life of the tube.

Also, from Eq. (31) the time required to wear is proportional to the contact angle κ by $[2\kappa - \sin(2\kappa)]$, and their relations are shown in Fig. 26. This can be expected from the fact that wide wear area is generated as a wear develops, and therefore more time is required to wear out the tube.

4. Conclusions

To investigate the vibration characteristics of helical tube, thermal-hydraulic and modal analyses for various conditions such as coil diameter, the number of turns and the number of supports etc are performed. The effects of modal characteristics on the fluidelastic instability are addressed. Also, derived in this study is the formula to predict the remaining life of the tube which is subject to fretting-wear by a foreign object. The time required to wear the tube is calculated based on the Archard's equation and several parameters are investigated for the effect on the life of the tube.

Based on the analyses performed, the following conclusions were derived:

(1) With the increasing coil diameter and the number of turns, the natural frequencies decrease and the changes are much more affected by the coil diameter than the number of turns.
(2) The optimal number of supports is found to be between 4 and 8 for each turn to avoid instability due to flow induced vibration.
(3) The natural frequency changes of the tube are negligible with the inclusion of the external pressure during a normal operation and therefore it can be concluded that fluidelastic instability and fretting-wear characteristics are not affected by the external pressure.
(4) Sufficient number of modes should be considered to calculate the time required to wear the tube.
(5) Type A and Type E are the worst tubes for the fluidelastic instability and fretting-wear point of views, respectively.

References

Au-Yang, M.K., 2001, *Flow-Induced Vibration of Power and Process Plant Components*, ASME Press, New York.

ANSYS, 2003, *ANSYS Structural Analysis Guide*, ANSYS, Inc., Houston.

Archard, J.F. and Hirst, T., 1956, "The Wear of Metals under Unlubricated Conditions," *Proceedings of the Royal Society of London*, Series A, Vol.236, p.397.

ASME, 1998, Flow-Induced Vibration of Tubes and Tube Banks, ASME Boiler and Pressure Vessel Code, Section III, Appendix N-1300, The American Society of Mechanical Engineers, New York.

Blevins, R.D., 1979, *Formulas for Natural Frequencies and Mode Shapes,* Van Nostrand Reinhold, New York.

CFX, 2003, *CFX-5.6 User Manual*, CFX Ltd., Oxfordshire, United Kingdom.

Connors, H.J., 1981, "Flow-Induced Vibration and Wear of Steam Generator Tubes," *Nuclear Technology*, Vol.55, pp.311-331.

Eisinger, F.L. and Juliano, T.M., 1975, *Flow-Induced Vibration Analysis of Recuperator Tube Bank*, 156-MA-75-48, Foster Wheeler Energy Corp., New Jersey.

Eisinger, F.L., Rao, M.S.M. and Steininger, D.A., 1989, "Numerical Simulation of Fluidelastic Instability of Multispan Tubes Partially Exposed to Cross Flow," *Proceedings of the10th International Conference on Structural Mechanics in Reactor Technology*, Vol.T, pp.45-57.

Jo, J.C., Jhung, M.J., Kim, W.S., Choi, Y.H., Kim, H.J. and Kim, T.H., 2003a, "Fretting-wear characteristics of steam generator tubes by foreign object," *Journal of the Korean Nuclear Society*, Vol.35, No.5, pp.442-453.

Jo, J.C., Jhung, M.J., Kim, W.S., Kim, H.J. and Kim, T.H., 2003b, "Vibration characteristics of steam generator U-tubes with defect," *Transactions of the Korean Society of Noise and Vibration Engineering*, Vol.13, No.5, pp.400-408.

Jo, J.C., and Shin, W.K., 1999, "Fluidelastic instability analysis of operating nuclear steam generator U-tubes," *Nuclear Engineering & Design*, Vol.193, No.1-2, pp.55-71.

Lindeburg, M.R., 1994, *Mechanical Engineering Reference Manual*, 9th ed., Professional Publications, Inc., Belmont.

Paidoussis, M.P., 1983, "A review of flow-induced vibrations in reactors and reactor components," *Nuclear Science Engineering*, Vol.74, pp.31-60.

Pettigrew, M. J., Carlucci, L. N., Taylor, C. E. and Fisher, N. J., 1991, "Flow-Induced Vibration and Related Technologies in Nuclear Components," *Nuclear Engineering and Design*, Vol.131, pp.81-100.

Pettigrew, M.J., and Gorman, D.J., 1981, "Vibration of heat exchanger tube bundles in liquid and two-phase cross-flow," *Flow-Induced Vibration Design Guidelines*, The American Society of Mechanical Engineers, New York, pp.89-110.

Pettigrew, M. J., Taylor, C. E., Fisher, N. J., Yetisir, M. and Smith, B.A.W., 1998, "Flow induced vibration : recent findings and open questions," *Nuclear Engineering and Design*, Vol.185, pp.249-276.

Yetisir, M. and Pettigrew, M.J., 2001, "A simple approach to estimate fretting-wear damage in heat exchanger tubes ; verification and validation," PVP-Vol.420.1, pp.7-16.

Table 1. Geometric description and material properties

Parameters	Type A	Type B	Type C	Type D	Type E
Wire diameter (mm)	10				
Wire thickness (mm)	1.5				
Coil diameter (mm)	422	338	282	198	142
Full height (mm)	1104	1150	1104	1104	1150
Number of turns	8	10	12	16	25
Young's modulus (Pa)	106.9E9				
Poisson's ratio	0.3				
Density (kg/m^3)	4490				

Table 2. Instability coefficients

Pitch layout	Triangle	Rotated traingle	Rotated square	Square	All arrays	Tube row
C_{mean}	4.5	4.0	5.8	3.4	4.0	9.5

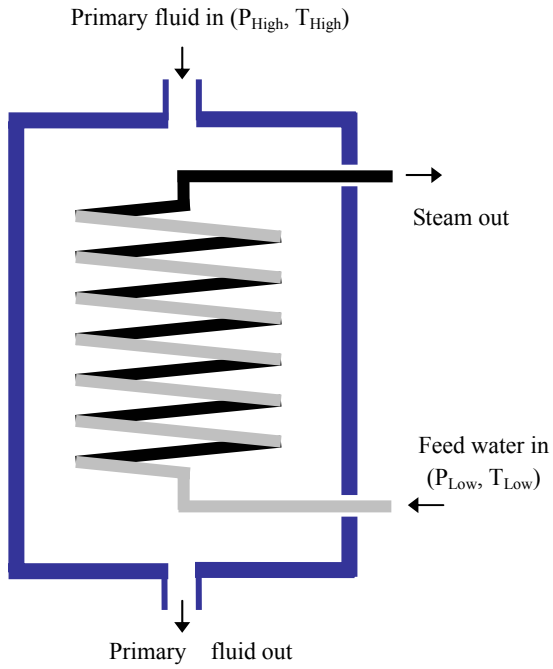

Figure 1. Schematic diagram of a helical coil steam generator

Figure 2. Helical coiled tube model for CFD analysis

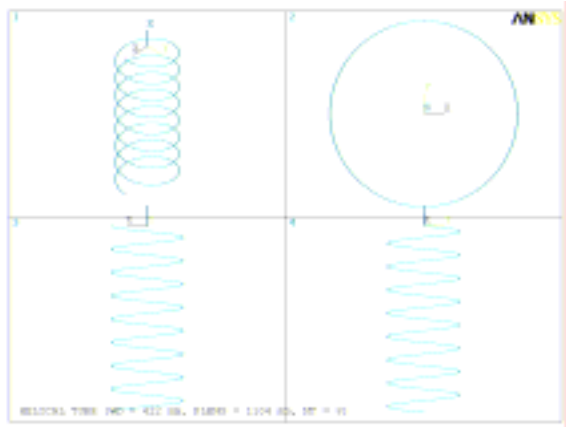

(a) Type A

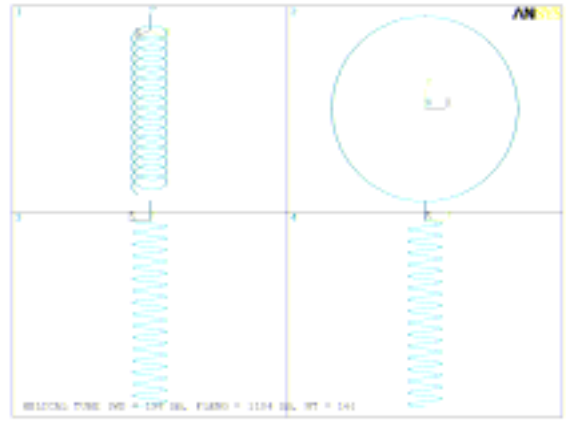

(d) Type D

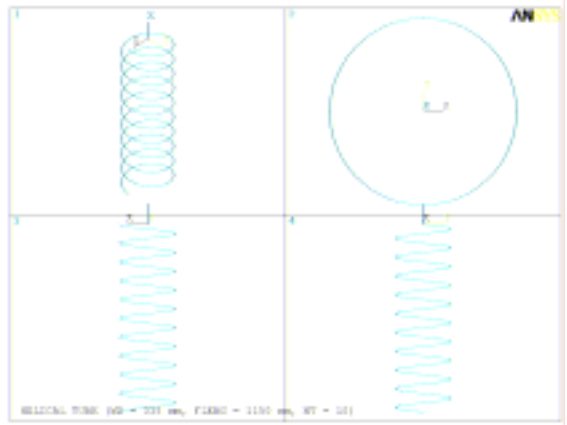

(b) Type B

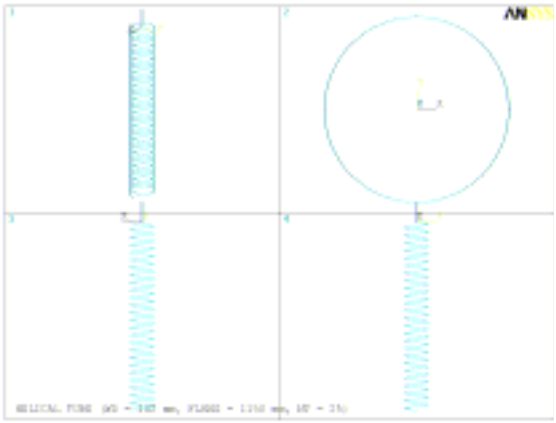

(e) Type E

Figure 3. Finite element models of helical tubes

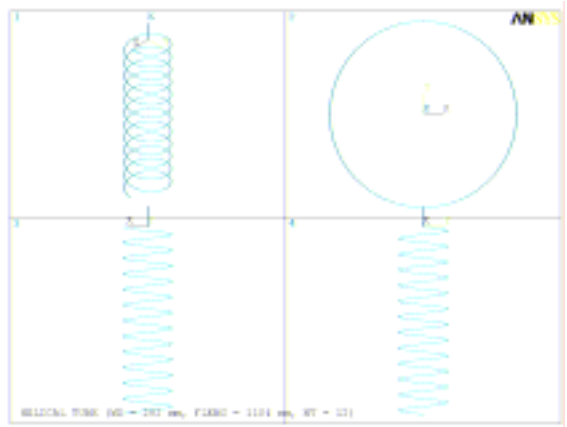

(c) Type C

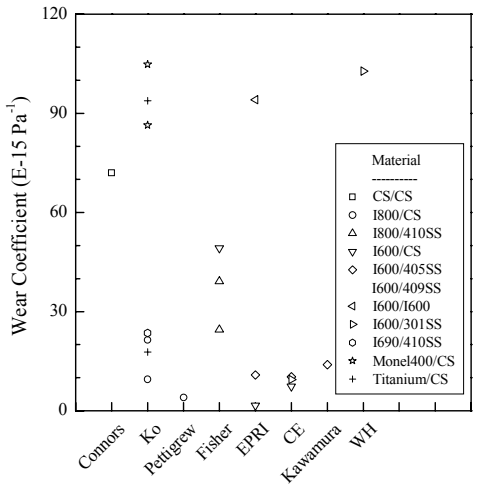

Figure 4. Wear coefficients for various material combinations

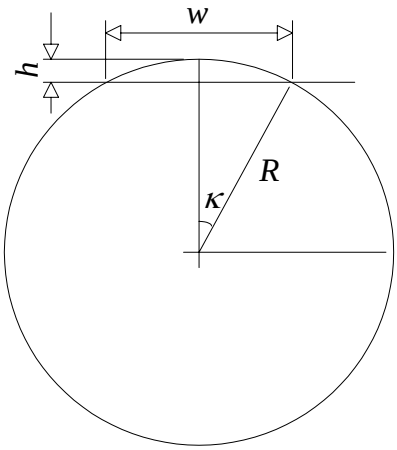

Figure 5. Contact between tube and flat bar

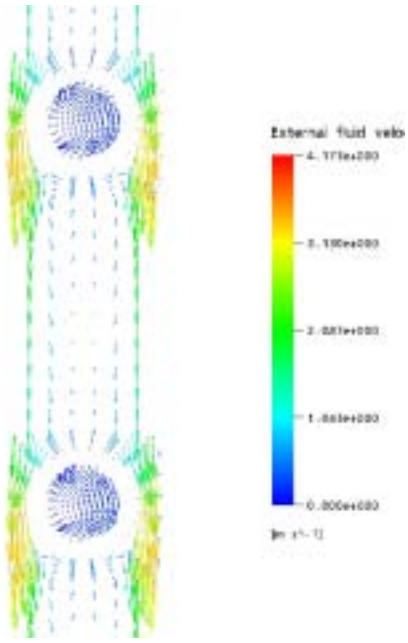

(a) external fluid

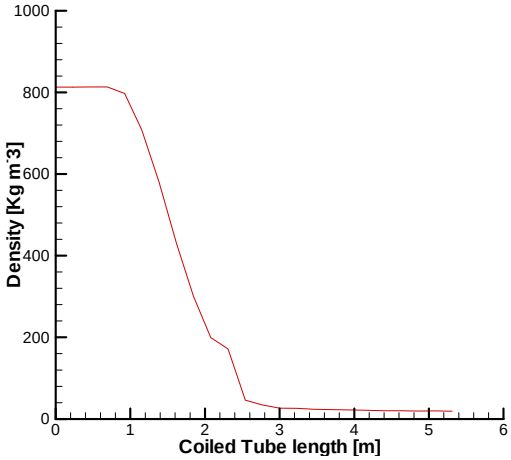

Figure 6. Typical density distribution of the internal fluid along the helically coiled tube

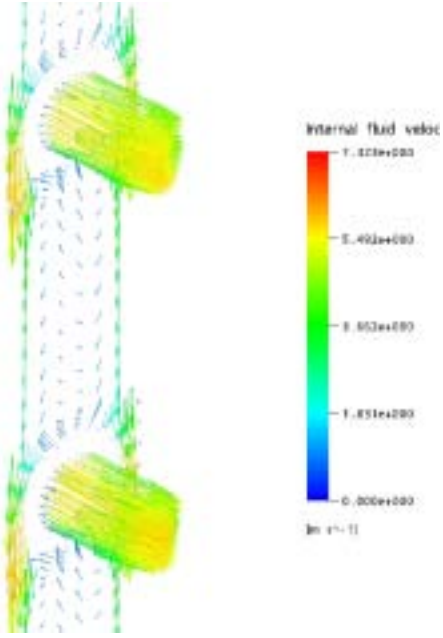

(b) internal fluid

Figure 7. Typical fluid velocity vectors at a cross-section of flow field

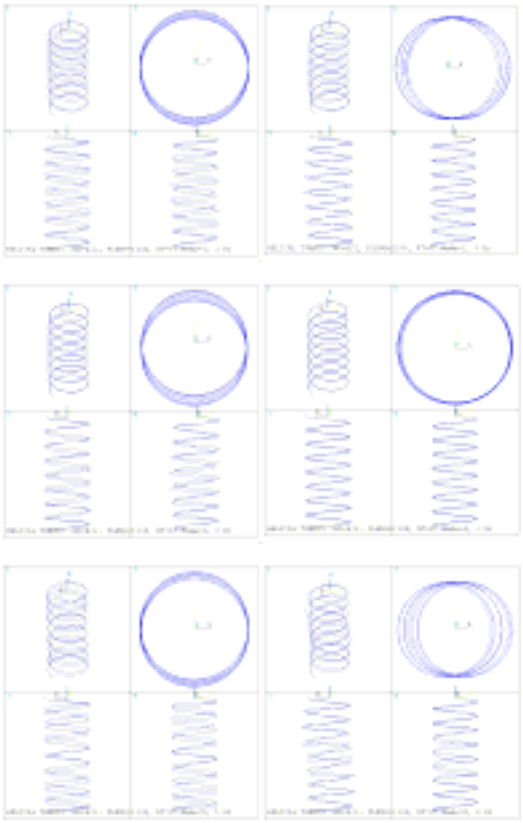

Figure 8. Typical mode shapes of helical tube without support

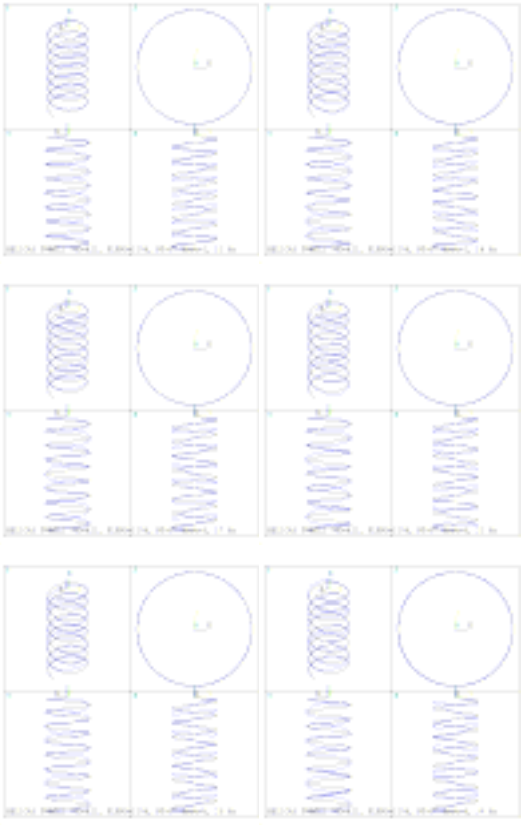

Figure 9. Typical mode shapes of helical tube with 2 supports

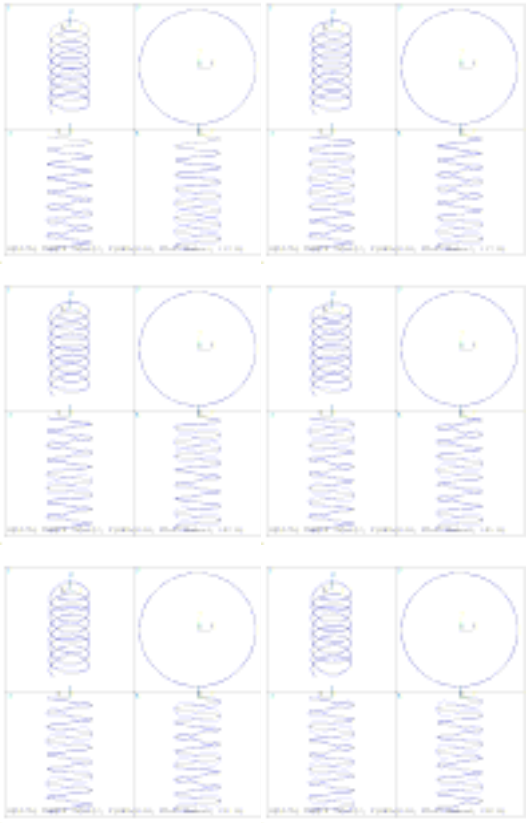

Figure 10. Typical mode shapes of helical tube with 4 supports

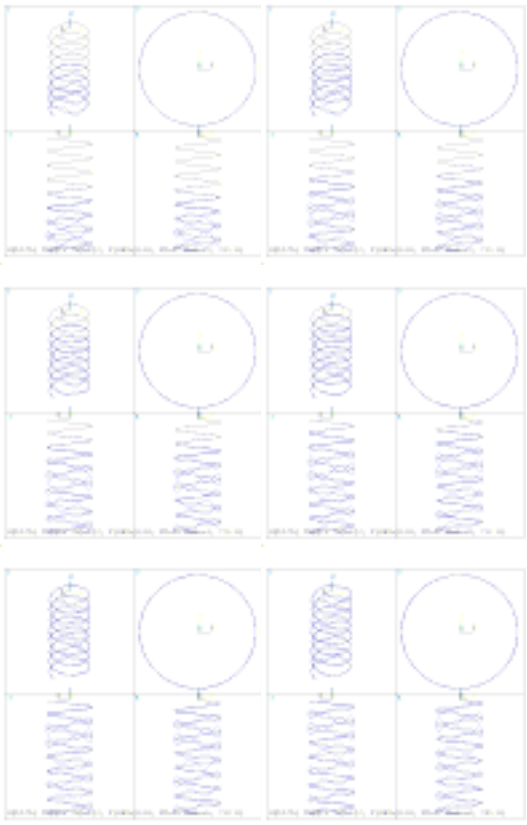

Figure 11. Typical mode shapes of helical tube with 8 supports

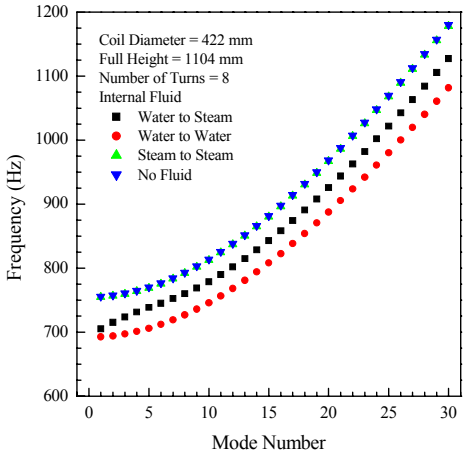

Figure 12. Natural frequency variations with respect to the status of internal fluid

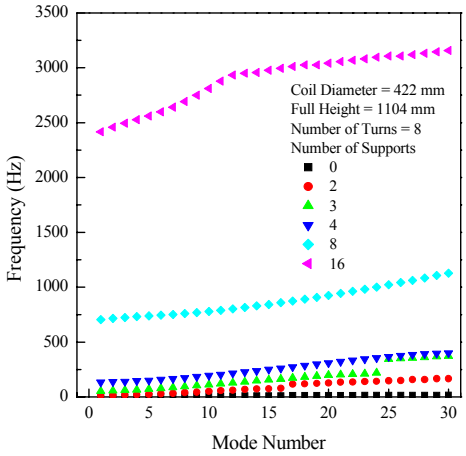

Figure 13. Natural frequency variations with respect to the number of supports

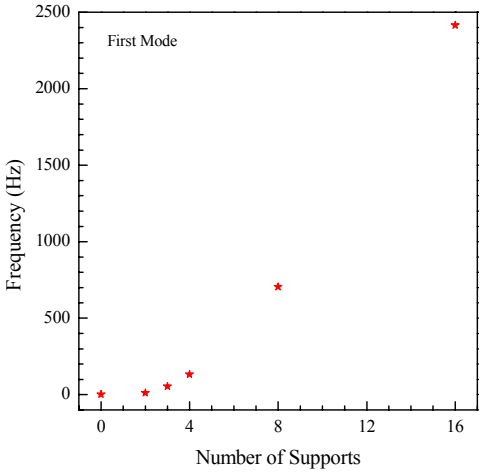

Figure 14. First mode frequency variations with respect to the number of supports

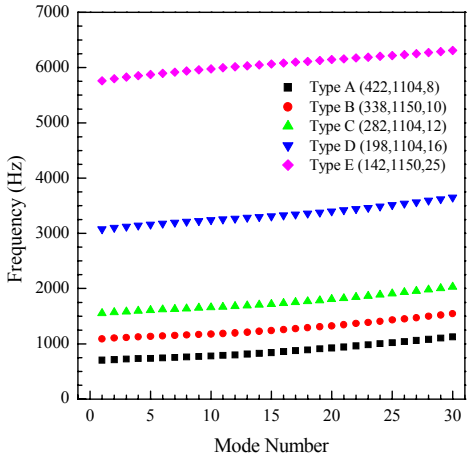

Figure 15. Natural frequency variations with respect to tube type

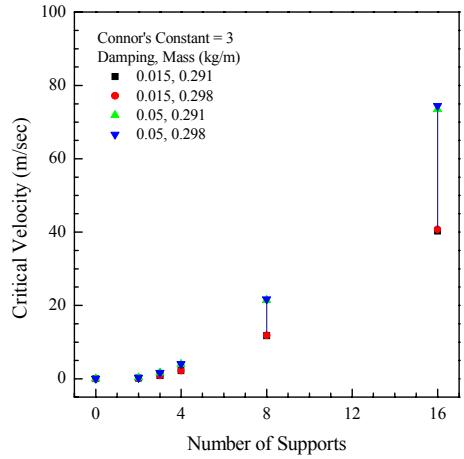

Figure 16. Critical velocity with respect to the number of supports

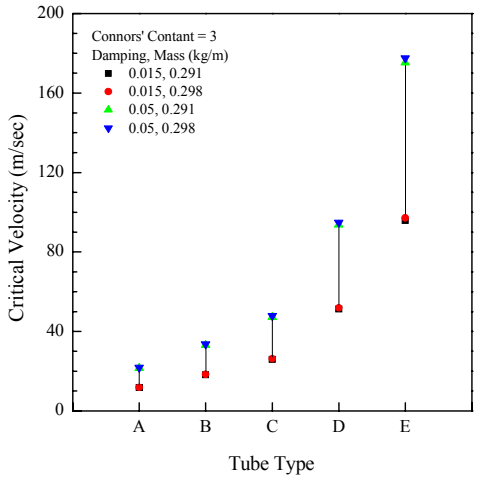

Figure 17. Critical velocity with respect to tube type

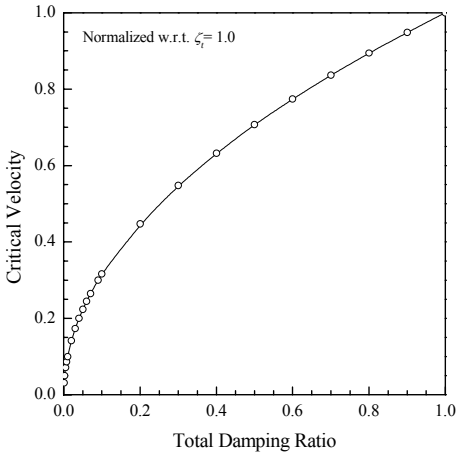

Figure 18. Critical velocity vs. total damping ratio

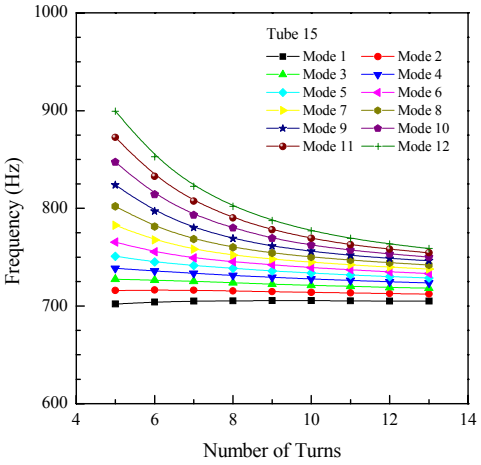

Figure 19. Natural frequency variations with respect to the number of turns

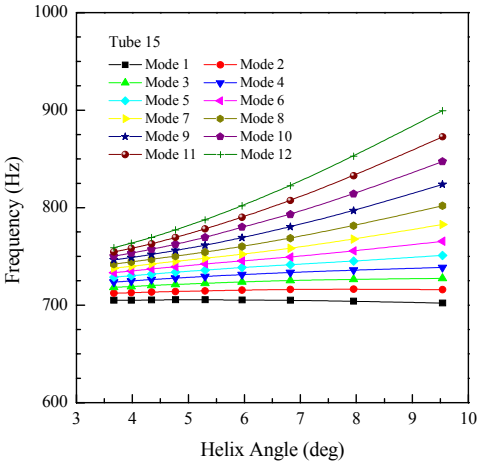

Figure 20. Natural frequency variations with respect to helix angle

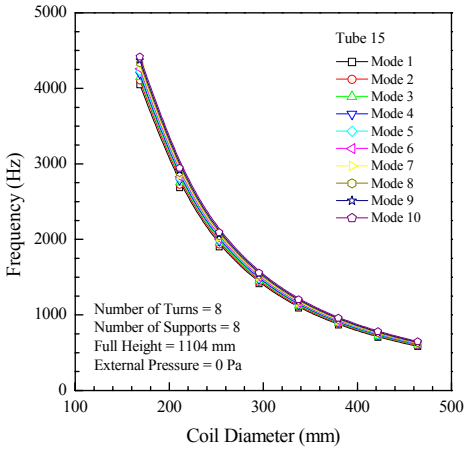

Figure 21. Natural frequency variations with respect to coil diameter

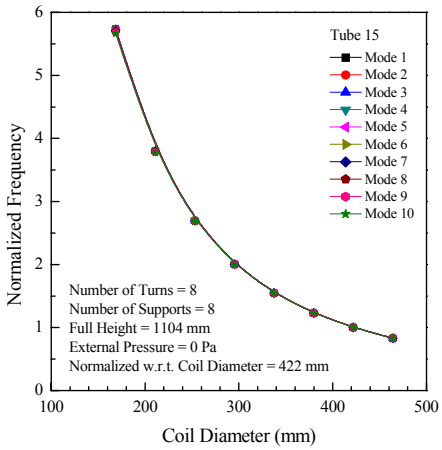

Figure 22. Normalized natural frequency variations with respect to coil diameter

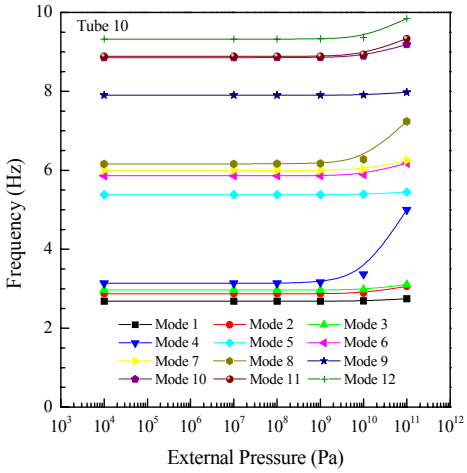

Figure 23. Natural frequency variations with respect to external pressure

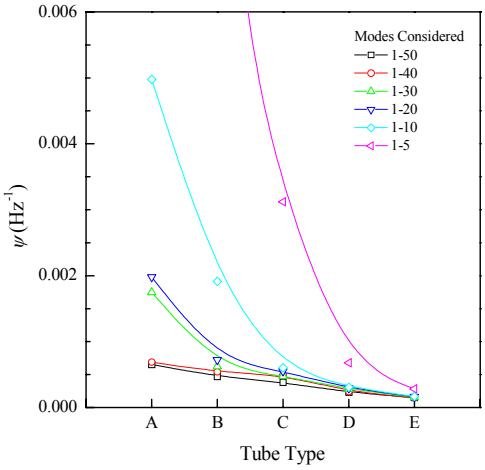

Figure 24. ψ according to tube type

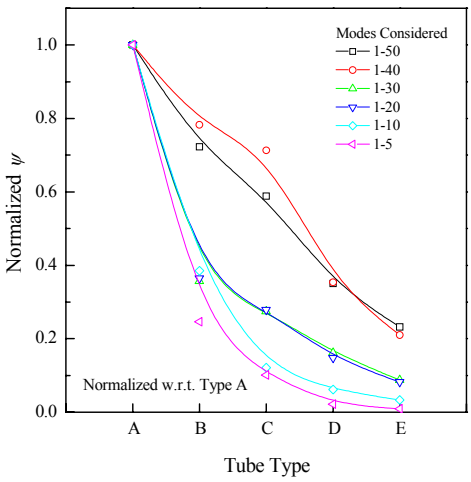

Figure 25. Normalized ψ with respect to tube Type A

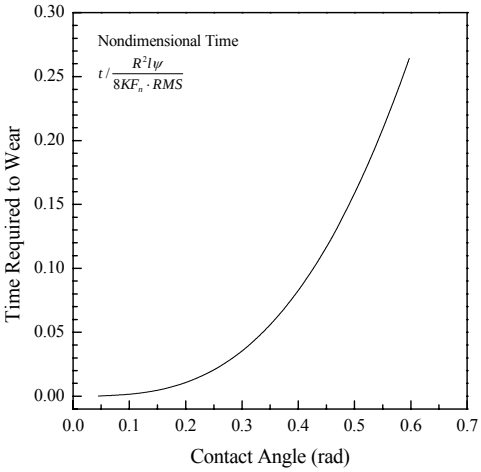

Figure 26. Time required to wear vs. contact angle